

# Geophysical Research Letters<sup>®</sup>






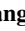



## RESEARCH LETTER

10.1029/2024GL114035

## Joint Observation of a Rotational Discontinuity by Tianwen-1 and MAVEN at Mars

### Key Points:

- We present the first joint observation of a rotational discontinuity at Mars using data from Tianwen-1 and MAVEN
- Based on the two-spacecraft joint analyses, we found that the discontinuity may be a curved structure
- The discontinuity has a thickness of  $\sim 9$  ion inertial lengths and carries a tangential current  $j \approx 12$  nA/m<sup>2</sup>

Z. Z. Guo<sup>1,2</sup> , H. S. Fu<sup>1,2</sup> , J. B. Cao<sup>1,2</sup> , Y. M. Wang<sup>3,4</sup> , M. Ge<sup>1,2</sup>, T. Y. Zhou<sup>1,2</sup>, W. D. Fu<sup>1,2</sup> , W. Z. Zhang<sup>1,2</sup> , and C. Q. Wang<sup>1,2</sup> 

<sup>1</sup>School of Space and Earth Sciences, Beihang University, Beijing, China, <sup>2</sup>Key Laboratory of Space Environment Monitoring and Information Processing, Ministry of Industry and Information Technology, Beijing, China, <sup>3</sup>Deep Space Exploration Laboratory/School of Earth and Space Sciences, University of Science and Technology of China, Hefei, China, <sup>4</sup>CAS Center for Excellence in Comparative Planetology/CAS Key Laboratory of Geospace Environment/Mengcheng National Geophysical Observatory, University of Science and Technology of China, Hefei, China

### Correspondence to:

H. S. Fu,  
[huishanf@gmail.com](mailto:huishanf@gmail.com)

### Citation:

Guo, Z. Z., Fu, H. S., Cao, J. B., Wang, Y. M., Ge, M., Zhou, T. Y., et al. (2025). Joint observation of a rotational discontinuity by Tianwen-1 and MAVEN at Mars. *Geophysical Research Letters*, 52, e2024GL114035. <https://doi.org/10.1029/2024GL114035>

Received 2 DEC 2024  
Accepted 10 MAR 2025

**Abstract** The solar wind plays a crucial role in the evolution of planets in the solar system, particularly Mars. Mars has no global intrinsic magnetic field, leading the solar wind to interact directly with the Martian ionosphere and atmosphere. However, there are many strong-current magnetic structures in the solar wind, which can directly affect the Martian induced magnetosphere and plasma environment. Using Tianwen-1 and MAVEN data, we present the first joint observation of a rotational discontinuity (RD) at Mars. The thickness of the RD is about 9 ion inertial lengths, and the tangential current density at the RD's center reaches  $\sim 12$  nA/m<sup>2</sup>. Based on the two-spacecraft joint analyses, we find that the RD may be a curved structure. These results can improve our understanding of Martian space environment.

**Plain Language Summary** The interaction between the solar wind and Mars has always been an open question. Usually, the solar wind carries a variety of magnetic structures, such as the discontinuity, which can directly interact with the Martian induced magnetosphere, thereby affecting the Martian space environment. In this study, using data from Tianwen-1 and MAVEN, we investigate the properties of a discontinuity at Mars. By analyzing the jumps in the magnetic field and plasma on both sides of the structure, we identify it as a rotational discontinuity (RD) and find that it also carries a strong current. Additionally, based on the two-spacecraft joint analyses, we speculate that the RD may be a curved structure.

## 1. Introduction

Mars has no global intrinsic magnetic field powered by active dynamo (e.g., Acuña et al., 1999), as a result, the expanding solar wind can directly interact with the Martian upper atmosphere and ionosphere, forming an induced magnetosphere (e.g., Nagy et al., 2004; Ramstad et al., 2020). On the other hand, there are some local areas on Mars with strong crustal magnetic fields, which can lead to the expansion of the ionosphere (Dubinin et al., 2020), deflect the solar wind (Fan et al., 2020), and affect the escape rates of planetary ions (e.g., Brain et al., 2010; Fang et al., 2010), etc., making the Martian space environment quite complex (e.g., Guo et al., 2024; Mazelle et al., 2004; Zhang et al., 1991). During the process of the solar wind-Mars interaction, a variety of interesting physical processes are triggered, such as planetary ion escape (e.g., Dong et al., 2015; Dubinin et al., 2011), magnetic field reconnection (e.g., Halekas et al., 2009; Harada et al., 2017, 2018), and the evolution of the induced magnetosphere (e.g., Guo et al., 2023; Xu et al., 2020). These processes are driven mainly by the solar wind.

In the solar wind, there are series of intermittent structures in the interplanetary magnetic fields, including discontinuities (e.g., Artemyev et al., 2018; Mariani et al., 1983; Smith, 1973), magnetic holes/peaks (e.g., Madanian et al., 2020), magnetic ropes (e.g., Cartwright & Moldwin, 2010). The interplanetary discontinuities are characterized by abrupt changes in the magnetic fields and/or the plasma properties. In magnetohydrodynamics framework, the Rankine-Hugoniot condition predicts the existence of four types of interplanetary discontinuities, including the shocks and contact/rotational/tangential discontinuities (Lin & Lee, 1993; Song & Russell, 1999). Among them, the rotational discontinuity (RD) is the most ubiquitous interplanetary discontinuities observed in the solar wind, and is identified by the magnetic fields and flow fields (e.g., Smith, 1973; Sonnerup et al., 2006). The RD carries transient currents which contribute significantly to the magnetic field fluctuation spectrum in the solar wind (e.g., Borovsky, 2010; Lion et al., 2016). The internal instabilities of the discontinuity are considered to be the reasons for magnetic field energy dissipation and corresponding acceleration and heating of charged

© 2025. The Author(s).

This is an open access article under the terms of the [Creative Commons Attribution-NonCommercial-NoDerivs License](https://creativecommons.org/licenses/by/4.0/), which permits use and distribution in any medium, provided the original work is properly cited, the use is non-commercial and no modifications or adaptations are made.

particles (e.g., Fu et al., 2011; Fu, Khotyaintsev, Vaivads, André, Sergeev, et al., 2012; MacBride et al., 2008; Tessein et al., 2013). The discontinuity carrying intense currents can be subject to the tearing instability (Cross & Van Hoven, 1971), which leads to magnetic reconnection (e.g., Uzdensky & Loureiro, 2016). What's more, in previous simulation study by Modolo et al. (2012), when a RD carried by the solar wind reaches the Martian space environment, the bow shock can adapt rapidly to the new solar wind conditions, and the magnetic lobes response to the new interplanetary magnetic field orientation after a few minutes. Therefore, the RD in solar wind upstream of planet can significantly affect the planetary space environment. But the observational studies of the RD in the Martian space environment have not been widely reported. Besides, due to the limitations of single-spacecraft observation, the characteristics of the RD have not been well understood yet, including shape features, real-time evolution and the effects on Martian induced magnetosphere.

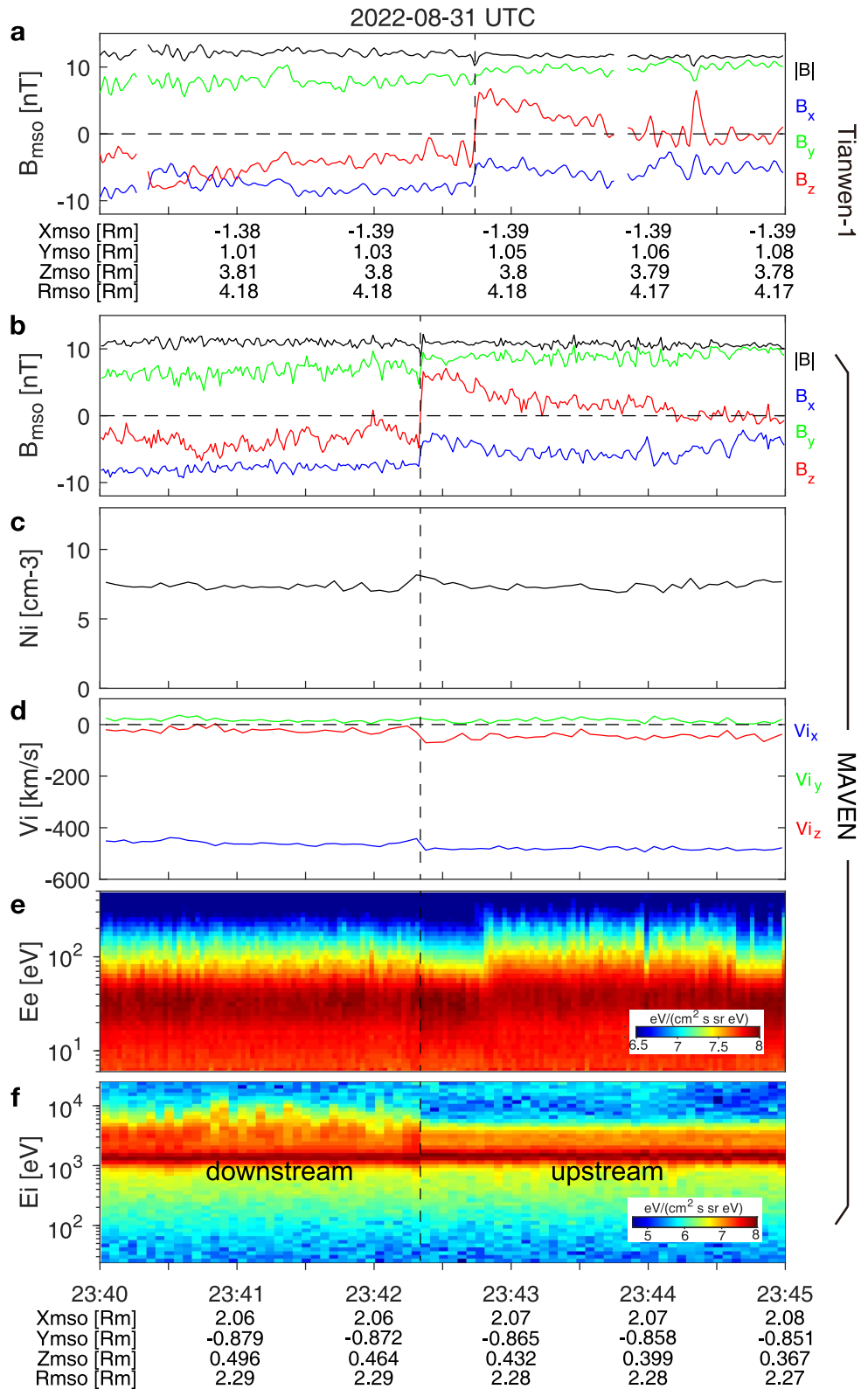
Here, the joint observation by Tianwen-1 (Wan et al., 2020) and MAVEN (Jakosky et al., 2015) provides an opportunity to study the RD at Mars in detail. In this study, we utilize simultaneous observations from Tianwen-1 and MAVEN to investigate the properties of a RD in the solar wind upstream of Mars.

## 2. Observation

We utilize data collected by the Tianwen-1 (Wan et al., 2020) and MAVEN (Jakosky et al., 2015) missions. Among them, the Mars Orbiter Magnetometer (MOMAG; Liu et al., 2020; Y. M. Wang et al., 2023; G. Q. Wang et al., 2024; Zou et al., 2023) on board the Tianwen-1 orbiter monitors the magnetic fields around Mars. In addition, the magnetic field, electron and ion data detected by MAVEN from Magnetometer (MAG; Connerney et al., 2015), Solar Wind Electron Analyzer instrument (SWEA; Mitchell et al., 2016) and Solar Wind Ion Analyzer instrument (SWIA; Halekas et al., 2015), respectively. Here, we use 1s resolution magnetic field measurements from MOMAG/Tianwen-1 and MAG/MAVEN, as well as 4s resolution proton moments provided by SWIA. The time resolution of electron spectrum is 2s. All the data are shown in Mars Solar Orbital (MSO) coordinates unless otherwise specified, in which X points from Mars toward the Sun, Z is perpendicular to the plane of the Martian heliocentric orbit and points northward, and Y completes the right-hand system.

We present a clear discontinuity event observed on 31 August 2022 in the Martian space environment. Figure 1 shows an overview of the discontinuity observed by Tianwen-1 and MAVEN in the solar wind. Figure 1a displays the magnetic field measured by Tianwen-1/MOMAG. We can clearly see that the  $B_z$  component quickly changes from  $-5$  to  $6$  nT at 23:42:44 UT, along with slight variations in the  $B_x$  component (from  $-7.8$  nT to  $-4.5$  nT) and the  $B_y$  component (from  $7.3$  to  $9.8$  nT). Meanwhile, the  $|B|$  remains essentially constant ( $\sim 11$  nT). These features indicate that the magnetic structure should be a discontinuity. We noticed that there is an apparent spike in the  $B_z$  component in Tianwen-1 measurements at 23:44:21 UT, which could be another discontinuity or a magnetic field perturbation. Here, we focus on the clear discontinuity. Interestingly, MAVEN also observed the same magnetic field structure 24s before (23:42:20 UT). Figures 1b–1f show the discontinuity measured by MAVEN. Specifically, the magnetic field (Figure 1b), ion density (Figure 1c), ion velocity (Figure 1d), the electron spectrum (Figure 1e) and ion spectrum (Figure 1f), are presented from top to bottom. At 23:42:20 UT, the signature of the discontinuity is evident (Figure 1b), with the  $B_z$  component quickly changing from  $-4.8$  to  $6.6$  nT, the  $B_x$  slightly decreasing from  $-7.5$  nT to  $-2.6$  nT, and the  $B_y$  slightly increasing from  $4.7$  to  $9.5$  nT. Throughout the entire period, the  $|B|$  remains almost constant at about  $11$  nT, consistent with Tianwen-1's observations (Figure 1a). The density remains constant on both the downstream (23:40:00–23:42:20 UT) and upstream (23:42:20–23:45:00 UT) sides of the discontinuity (Figure 1c), ruling out the possibility of tangential discontinuity (e.g., Fu, Chen, et al., 2020; Fu, Grigorenko, et al., 2020; Fu, Zhao, et al., 2020; Fu et al., 2022; Guo et al., 2021; Xu et al., 2019, 2021). Moreover, the  $V_z$  component of the ion velocity slightly increases (Figure 1d). The electron and ion spectra in Figures 1e and 1f also show distinct particle properties on the downstream and upstream sides of the discontinuity. It can be seen that the ion fluxes above  $4$  keV are higher downstream of the discontinuity, whereas the electron fluxes above  $100$  eV are higher upstream. It is worth mentioning that the electron fluxes decrease during 23:42:20–23:42:50 UT upstream of the discontinuity. The similar phenomenon—electron flux decrease was detected again during 23:44:38 to 23:44:58 UT, but the corresponding physical mechanism is currently unclear. We will investigate this issue in future work. In this paper, we focus on studying the discontinuity. The electron moments are not shown here due to the influence of spacecraft potential.

Figure 2a illustrates the Tianwen-1 and MAVEN positions in  $X_{\text{MSO}}-\rho$  plane. During 23:40:00–23:45:00 UT, MAVEN was located near  $[2.06 -0.87 0.44]R_M$  ( $R_M$  is Martian radii,  $\sim 3389.5$  km) in the solar wind upstream of



**Figure 1.** Overview of the event of a discontinuity measured by Tianwen-1 and MAVEN on 2022 August 31. Observations from 23:40 to 23:45 UT, including Tianwen-1 observations of (a) the magnetic field, MAVEN observations of (b) the magnetic field, (c) the proton density, (d) the ion velocity, the electrons (e) and ions (f) spectra. Mars Solar Orbital = MSO.

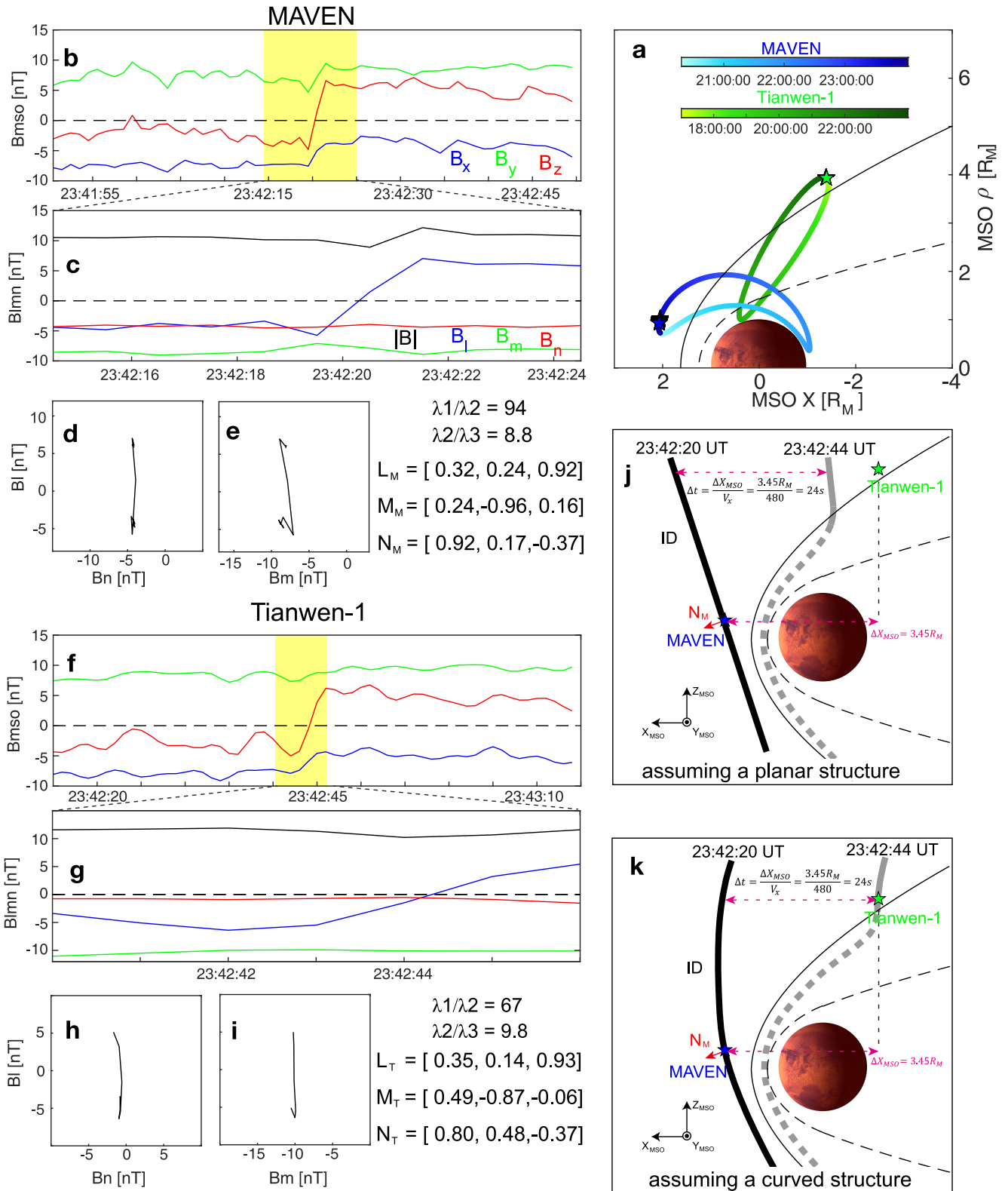
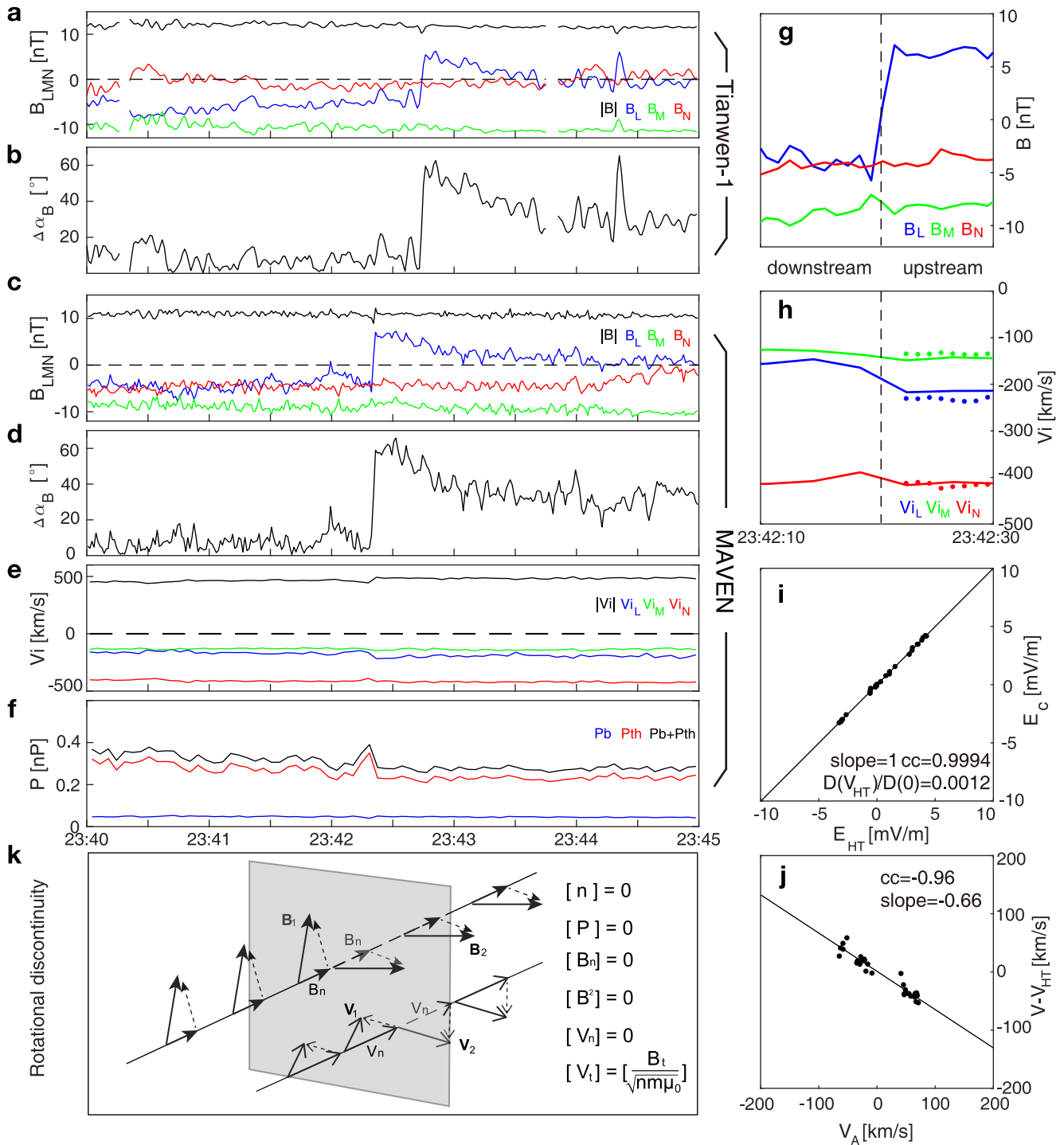


Figure 2.

Mars, while Tianwen-1 was situated in the northern solar wind of Mars at approximately  $[-1.39 \ 1.03 \ 3.80]R_M$  (the pentacles in Figure 2a). Thus, MAVEN observed the discontinuity first (Figure 1). The distance between the two spacecraft in the  $X_{MSO}$  direction is about  $3.45 R_M$ , and the solar wind velocity  $V_x$  component is close to  $-480$  km/s (Figure 1d). It is estimated that the time difference  $\Delta t$  of the discontinuity measured by two spacecraft is about 24s, consistent with the results of Figures 1a and 1b. This suggests that MAVEN and Tianwen-1 observed the same discontinuity. We applied minimum variance analysis (MVA) to the discontinuity to determine its normal direction (Cao et al., 2013; Mazelle et al., 1997; Sonnerup & Cahill, 1968). For MAVEN's crossing, MVA was applied from 23:42:14.498 to 23:42:25.037 UT (the yellow shaded area in Figure 2b). The resulting intermediate-to-minimum eigenvalue ratio is  $\lambda_2/\lambda_3 = 8.8$  (whereas  $\lambda_1/\lambda_2 = 94$ ), indicating that the minimum variance vector can be deemed as acceptable. We thus obtained a local coordinate system LMN-MAVEN,  $L_M = [0.32, 0.24, 0.92]$ ,  $M_M = [0.24, -0.96, 0.16]$ , and  $N_M = [0.92, 0.17, -0.37]$  in MSO coordinates. Here, L denotes the maximum variance of magnetic field during the process of crossing the discontinuity, N is normal to the discontinuity, and M completes the right-hand coordinate system. Figure 2c displays the magnetic field in LMN coordinate system, where the  $|B|$ ,  $B_M$  and  $B_N$  remain essentially constant, while  $B_L$  reverses from  $-5$  to  $6$  nT. This reveals that the direction of magnetic field rotates in the tangential (L-M) plane after crossing the discontinuity. In Figures 2d and 2e, two hodograms describe the magnetic field components along the maximum and minimum variance directions ( $B_L$  and  $B_N$ ) and the maximum and intermediate variance directions ( $B_L$  and  $B_M$ ) between 23:42:14.498 and 23:42:25.037. For Tianwen-1's crossing, we performed the MVA on the magnetic field during 23:42:40 to 23:42:46 UT (see the yellow shaded area in Figure 2f) to obtain a local coordinate system LMN-Tianwen-1. With respect to the MSO coordinates,  $L_T = [0.35, 0.14, 0.93]$ ,  $M_T = [0.49, -0.87, -0.06]$ , and  $N_T = [0.80, 0.48, -0.37]$ . The resulting intermediate-to-minimum eigenvalue ratio is  $\lambda_2/\lambda_3 = 9.8$  (whereas  $\lambda_1/\lambda_2 = 67$ ), indicating that the minimum variance vector can be deemed as acceptable. Similarly, these characteristics of magnetic fields are presented in Figures 2g–2i and are consistent with the MAVEN observations. However, the normal directions of the discontinuity are different in the two observations. Here, we proceed to analyze the shape of the discontinuity (Figures 2j and 2k). We first assume that the discontinuity is a planar shape. Combined with the normal direction  $N_M$  ( $0.92, 0.17, -0.37$ ) calculated by MAVEN, we can outline its contour in Figure 2j with the black thick line. During its propagation along the  $-X_{MSO}$  direction, certain localized regions may interact with the Martian induced magnetosphere, while other parts in the solar wind continue to propagate at solar wind speed. In this scenario, the discontinuity cannot reach the position of Tianwen-1 after 24s, as illustrated by the gray thick line in Figure 2j. However, if the initial discontinuity is a curved shape (Figure 2k), it could potentially reach the location of Tianwen-1 24s after being observed by MAVEN. Therefore, we are more inclined to the possibility of curved discontinuity. In addition, the two normal directions are not collinear, possibly due to the interaction between the discontinuity and Mars or its inherently curved shape.

In Figure 3, we further analyze the properties of the discontinuity. Figure 3a shows the magnetic field in the  $L_T$ ,  $M_T$  and  $N_T$  directions measured by Tianwen-1. As can be seen, the  $B_M$  and  $B_N$  components, as well as  $|B|$ , remain constant upstream and downstream of the discontinuity, while the  $B_L$  component exhibits a reversal. Furthermore, the  $B_N$  component is quite small compared with the magnetic field magnitude, indicating that the mean magnetic field is nearly tangential. As a result, the magnetic field lies mainly in the L-M plane, where it describes a rotation. Based on the background magnetic field (23:40:00–23:42:00 UT) downstream of the discontinuity, we calculated the rotation angle of the magnetic field while crossing the discontinuity, about  $60^\circ$  (Figure 3b), meaning that such discontinuity may be a RD (e.g., Burlaga, 1971). These features of magnetic field are the same as those observed by MAVEN (see Figures 3c and 3d) and will not be repeated here. We can obtain the jump relations of the magnetic field across the discontinuity:  $[B_N] = 0$  and  $[B^2] = 0$ ; the square bracket “[ ]” indicates the jump of the physical quantity on both sides of the discontinuity. Figure 3e displays the  $L_M$ ,  $M_M$ ,  $N_M$  components of the velocity and total velocity observed by MAVEN, it can be seen that the normal component  $V_{iN}$  is almost constant,

**Figure 2.** The positions of two spacecraft and minimum variance analysis (MVA) analyses. (a) Tianwen-1 and MAVEN positions in  $X_{MSO}$ - $\rho$  plane,  $\rho = (Y_{MSO}^2 + Z_{MSO}^2)^{1/2}$ . The solid and dashed lines mark the bow shock and magnetic pileup boundary models based on Trotignon et al. (2006). The blue and green trajectories indicate a full orbit of MAVEN and Tianwen-1, respectively, and the pentacle presents the position of spacecraft during 23:40:00–23:45:00 UT. (b) MVA is applied to the magnetic field observed by MAVEN (yellow shaded area), the results including (c) the magnetic field in the L, M and N directions, the magnetic field components along the maximum and minimum variance directions (d) and maximum and intermediate variance directions (e). (f–i) The MVA results of Tianwen-1 observations have the same format with (b–e) panels. (j, k) The results of the analysis of discontinuity shape;  $N_M$  = the normal direction of discontinuity calculated by MAVEN, ID = interplanetary discontinuity; the thick lines indicate discontinuity.



**Figure 3.** Identification of the RD. (a) Tianwen-1 magnetic field data in  $L_T M_T N_T$  coordinates, (b) the angles of magnetic field rotation. MAVEN measurements of (c) the magnetic field in  $L_M M_M N_M$  coordinates, (d) the angles of magnetic field rotation. (e) the ion velocity in  $L_M M_M N_M$  coordinates and (f) the pressure (magnetic pressure, proton thermal pressure and the sum). (g, h) The jump conditions across the RD. In panel (h), the solid lines present the actual upstream and downstream velocities, while the dots show the theoretical upstream velocity to satisfy the Walén relation. (i, j) Walén test for the RD. (k) A schematic illustrating idealized RD; the square bracket “[ ]” indicates the jump of the physical quantity on both sides (upstream and downstream) of the discontinuity.

that is,  $[V_{iN}] = 0$ . In addition, the ion density remains continuous, that is,  $[n] = 0$  (Figure 1c). Figure 3f displays the proton thermal pressure, the magnetic pressure and the sum. For the RD, the total pressure should be continuous ( $[P] = 0$ ); however, the sum of proton thermal pressure and magnetic pressure is slightly higher

downstream of the RD than upstream. This discrepancy may result from not accounting for the contribution of electrons.

The strongest evidence for identifying the RD may be the Walén relation (e.g., Sonnerup et al., 2018), which limits the jumps in the tangential component of the velocity and magnetic field crossing the RD by  $[V_t] = [B_t/\sqrt{nm\mu_0}]$ . For the discontinuity observed by MAVEN, we show the field jump conditions in Figure 3g, and the velocity jump conditions are presented by the solid curves in Figure 3h. We calculate the velocity changes  $[\Delta V]$  crossing the discontinuity from the magnetic field changes by the Walén relation, and then add  $[\Delta V]$  to the downstream velocity to estimate the theoretical upstream velocity. The results are presented in Figure 3h by the dots. It can be seen that the actual velocity change agrees well with the theoretical results. Additionally, we also perform a standard test (Walén test) for a deHoffman-Teller frame (DeHoffmann & Teller, 1950) on the MAVEN data between 23:42:00 and 23:42:40 UT. To avoid errors caused by interpolation, the magnetic field data (1s) were downsampled to 4s to match the time resolution of ion velocity during the analysis. The results are shown in Figures 3i and 3j. The frame velocity vector,  $V_{HT}$ , can be estimated from a set of measurements of plasma bulk velocity,  $v^m$ , and magnetic field,  $B^m$ ,  $m = 1, 2 \dots M$ . We may seek a reference frame in which the mean square of the electric field is as small as possible. The mean square is

$$D(V) = \frac{1}{M} \sum_{m=1}^M |(v^m - V) \times B^m|^2.$$

The  $V_{HT}$  is the value of the frame velocity,  $V$ , that minimizes  $D$ . In our case, applying the formula  $D(V)$  to this time interval (23:42:00-23:42:40 UT) gives the components of  $V_{HT}$  in MSO coordinates:  $V_{HT} = (-500, 57, -31)$  km/s. Then, the two electric fields  $E_c^m = -v^m \times B^m$  and  $E_{HT}^m = -V_{HT} \times B^m$  are calculated against each other, component by component, in Figure 3i. The correlation between these two fields is excellent (with a high correlation coefficient of 0.9994), and the ratio  $D(V_{HT})/D(0)$  is about 0.0012, indicating existence of a good deHoffman-Teller frame. Figure 3j illustrates the relation between  $v^m - V_{HT}$  and  $V_A$ , where  $v^m - V_{HT}$  is the plasma velocity in the deHoffman-Teller frame, and  $V_A$  is the Alfvén velocity. The linear fit of  $v^m - V_{HT}$  versus  $V_A$  data shows a good linear relationship, indicating that the Walén relation is satisfied and that the structure is a RD (e.g., J. Wang et al., 2008), as depicted in the schematic diagram of Figure 3k.

In general, the RD is considered as a current sheet carrying an intense current (e.g., Artemyev et al., 2020). According to the Maxwell-Ampere law,  $\mu_0 \mathbf{J} = \nabla \times \mathbf{B}$ , we can estimate the local current density  $\mathbf{J}$ , expanded as follows:

$$\mathbf{J} = \frac{1}{\mu_0} \nabla \times \mathbf{B} = \frac{1}{\mu_0} \begin{vmatrix} \hat{l} & \hat{m} & \hat{n} \\ \frac{\partial}{\partial l} & \frac{\partial}{\partial m} & \frac{\partial}{\partial n} \\ B_l & B_m & B_n \end{vmatrix} = \frac{1}{\mu_0} \left[ \left( \frac{\partial B_n}{\partial m} - \frac{\partial B_m}{\partial n} \right) \hat{l} + \left( \frac{\partial B_l}{\partial n} - \frac{\partial B_n}{\partial l} \right) \hat{m} + \left( \frac{\partial B_m}{\partial l} - \frac{\partial B_l}{\partial m} \right) \hat{n} \right],$$

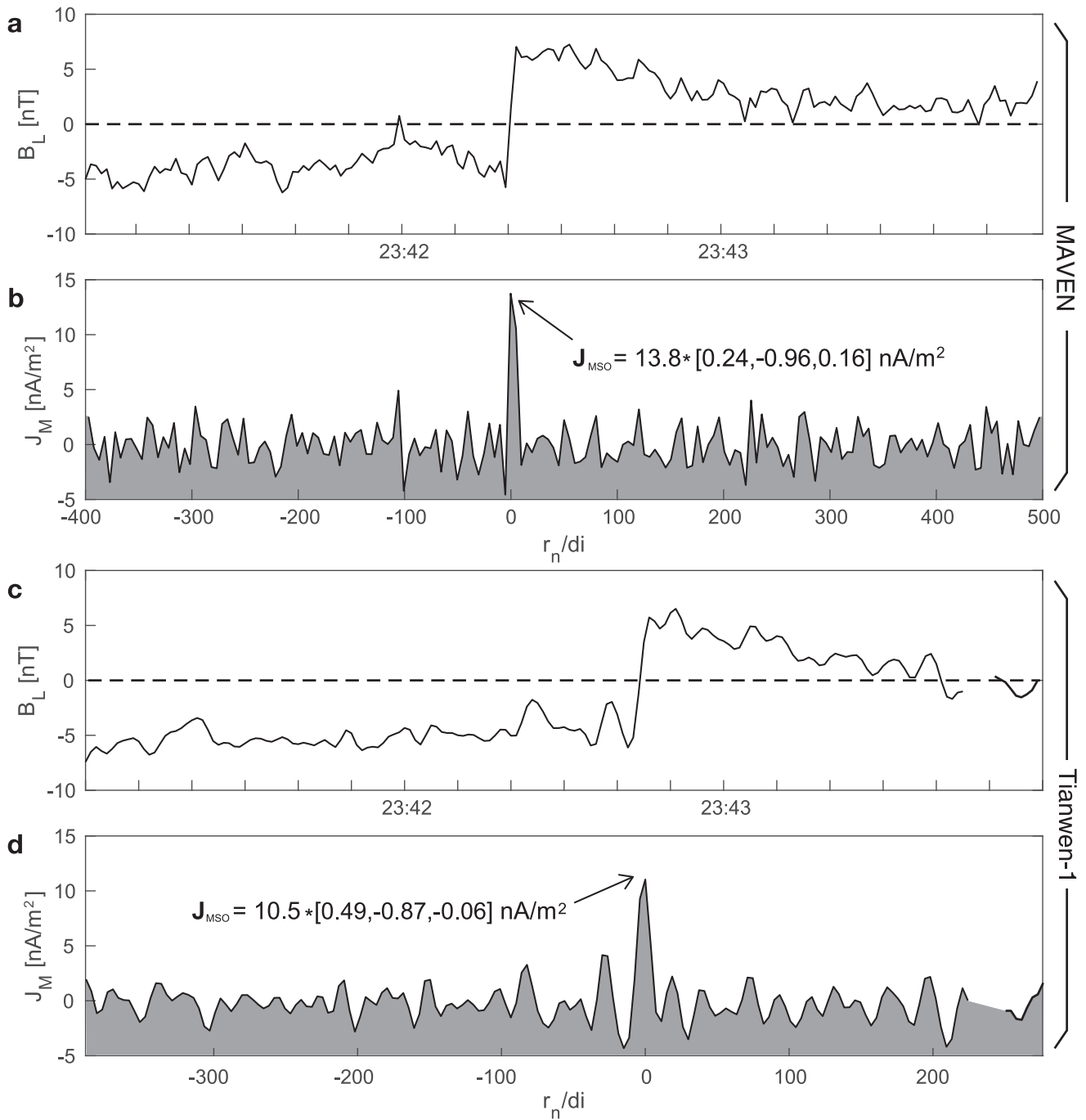
where  $\mu_0$  is the permeability in vacuum. Then the  $\mathbf{m}$  component of current density is

$$J_m = \frac{1}{\mu_0} \left( \frac{\partial B_l}{\partial n} - \frac{\partial B_n}{\partial l} \right) \approx \frac{1}{\mu_0} \left( \frac{\partial B_l}{\partial t} \frac{\partial t}{\partial n} - \frac{\partial B_n}{\partial t} \frac{\partial t}{\partial l} \right).$$

Since the  $B_n$  component of magnetic field remains stable while crossing the RD, so the second team,  $\frac{\partial B_n}{\partial t} \frac{\partial t}{\partial l}$ , can be neglected. Therefore, the  $J_m$  can be simplified to

$$J_m \approx \frac{1}{\mu_0} \left( \frac{\partial B_l}{\partial t} \frac{\partial t}{\partial n} \right) \approx \frac{1}{\mu_0} \frac{\partial B_l}{v_n \partial t}.$$

This formula has also been widely used in previous studies (e.g., Artemyev et al., 2018; Fu, Khotyaintsev, Vaivads, André, & Huang, 2012). Knowing the normal direction  $\mathbf{n}$ , we can project the solar wind velocity  $v_n = \mathbf{v} \cdot \mathbf{n}$  and calculate the spatial scale across discontinuity  $r_n = \int v_n dt$ . This allows us to estimate current



**Figure 4.** The local current density. Top two rows (a, b): MAVEN observations; bottom two rows (c, d): Tianwen-1 observations. The  $B_L$  components of the magnetic field (a, c); the current density  $J_M$  (b, d) as a function of normalized distance,  $r_n/d_i$ .

density  $J_M$  across the discontinuity, as shown in Figure 4. Figures 4a and 4b shows the MAVEN observations. It can be seen that  $J_M$  peaks at the RD's center and reaches  $13.8 \text{ nA/m}^2$  (see Figure 4b). The thickness of RD can be estimated as  $L \approx \frac{\max B_L - \min B_L}{\mu_0 \max J_M}$  (Artemyev et al., 2018; Webster et al., 2021). In this estimation, based on MAVEN observations, we estimate the thickness of the RD to be approximately 8.8 ion inertial lengths ( $d_i = \frac{c}{\omega_{pi}}$ , where  $c$  is the speed of light and  $\omega_{pi}$  is the proton plasma frequency; here  $1 d_i \approx 83 \text{ km}$ , corresponding to the proton density of  $7.5 \text{ cm}^{-3}$ , see Figure 1c). Because Tianwen-1 is also in the solar wind, assuming solar wind speed is quasi-stationary on the scale of observations, we can estimate the current density and thickness at the local region



where Tianwen-1 crosses the RD, as shown in Figures 4c and 4d. The  $B_L$  component changes from  $-6.3$  to  $5.4$  nT (Figure 4c) when Tianwen-1 crosses the RD. In the same way, we estimated the current density at the RD's center to be  $10.5$  nA/m<sup>2</sup> (see Figure 4d), and the local thickness is about  $10.6 d_i$ .

### 3. Discussion

In this study, the thickness of the RD calculated by MAVEN is  $8.8 d_i$ , which is very close to the result of Tianwen-1 ( $10.6 d_i$ ), indicating that its thickness may be relatively uniform. In previous single spacecraft statistical studies (e.g., Artemyev et al., 2018), typical discontinuity thickness around Mars varies mainly between 1 and 20 ion inertial lengths, and the current intensities  $J_M$  are mainly concentrated in the range of  $0.1$ – $10$  nA/m<sup>2</sup>. The discontinuity thickness is in good agreement with our observations, but the current density in the present study is stronger, about  $12$  nA/m<sup>2</sup>. Moreover, one of the key advantages of two-spacecraft observations is the ability to analyze the shape and evolution of the discontinuity. Based on the normal directions of discontinuity and the time difference between Tianwen-1 and MAVEN observing the RD, we speculate that the shape of the RD could be actually curved rather than planar.

In addition, MAVEN is located near the upstream of subsolar bow shock, while Tianwen-1 is situated in the north flank of the bow shock (see Figure 2a). When Tianwen-1 observed the RD, it had likely already interacted with Mars. During the interaction, the discontinuity carrying a strong current may affect the magnetic field fluctuation spectrum and energy transfer ( $E \cdot J$ ) in the induced magnetosphere, as well as alter the magnetic lobes configuration. The previous simulation study reported that when the RD conveyed by the solar wind reached the Martian environment the magnetic lobes configuration adjusted to the new interplanetary magnetic field after about one hundred seconds (Modolo et al., 2012). Here, the curved shape of the RD could significantly affect the response time of the Martian plasma environment to it. Unfortunately, Tianwen-1 did not detect the response of the Martian magnetosphere due to being located in the solar wind. The response of the Martian magnetosphere to interplanetary discontinuities will be presented in our future work.

### 4. Conclusion

In this letter, we presented the first joint observation of a RD at Mars by using Tianwen-1 and MAVEN data. Through MVA analysis, we found that the discontinuity has the typical properties of the RD, including continuous density, total magnetic field, normal magnetic field, and normal velocity, etc. Crossing the discontinuity, the direction of the magnetic field rotates about  $60^\circ$  around the local normal direction, and the Walén relation was also confirmed to be satisfied. Therefore, we identify the discontinuity as a RD. The thickness of such RD is estimated to be  $\sim 9$  ion inertial lengths, and the tangential current at the RD's center reaches  $\sim 12$  nA/m<sup>2</sup>. Based on the two-spacecraft joint analyses, we found that the shape of the RD may be curved.

### Data Availability Statement

The Tianwen-1/MOMAG data used in this study are publicly available at (Y. M. Wang, 2024) [https://space.ustc.edu.cn/dreams/tw1\\_momag/?magdata=cal](https://space.ustc.edu.cn/dreams/tw1_momag/?magdata=cal). The MAVEN MAG, SWEA, SWIA data used in this study are available at (Connerney, 2024) <https://doi.org/10.17189/1414251>, (Mitchell, 2024) <https://doi.org/10.17189/1414254>, and (Halekas, 2024) <https://doi.org/10.17189/1414248>, respectively.

### References

- Acuña, M., Connerney, J., Ness, N. F., Lin, R. P., Mitchell, D., Carlson, C. W., et al. (1999). Global distribution of crustal magnetization discovered by the Mars Global Surveyor AG/ER experiment. *Science*, *284*(5415), 790–793. <https://doi.org/10.1126/science.284.5415.790>
- Artemyev, A. V., Angelopoulos, V., Halekas, J. S., Vinogradov, A. A., Vasko, I. Y., & Zelenyi, L. M. (2018). Dynamics of intense currents in the solar wind. *The Astrophysical Journal*, *859*(2), 95. <https://doi.org/10.3847/1538-4357/aabe89>
- Artemyev, A. V., Angelopoulos, V., Vasko, I. Y., & Zelenyi, L. M. (2020). Ion nongyrotropy in solar wind discontinuities. *The Astrophysical Journal Letters*, *889*(1), L23. <https://doi.org/10.3847/2041-8213/ab6b2e>
- Borovsky, J. E. (2010). Contribution of strong discontinuities to the power spectrum of the solar wind. *Physical Review Letters*, *105*(11), 111102. <https://doi.org/10.1103/PhysRevLett.105.111102>
- Brain, D. A., Baker, A. H., Briggs, J., Eastwood, J. P., Halekas, J. S., & Phan, T.-D. (2010). Episodic detachment of Martian crustal magnetic fields leading to bulk atmospheric plasma escape. *Geophysical Research Letters*, *37*(14), L14108. <https://doi.org/10.1029/2010GL043916>
- Burlaga, L. F. (1971). Nature and origin of directional discontinuities in the solar wind. *Journal of Geophysical Research*, *76*(19), 4360–4365. <https://doi.org/10.1029/JA076i019p04360>

### Acknowledgments

We would like to thank the Tianwen-1 and MAVEN team for providing data access and support. Special thanks to J. E. P. Connerney, D. L. Mitchell and J. S. Halekas for their contributions in making available data from MAG, SWEA, and SWIA, respectively. This work was supported by NSFC Grants 42241113. The calibration of MOMAG data is supported by NSFC 42130204.

- Cao, J. B., Wei, X. H., Duan, A. Y., Fu, H. S., Zhang, T. L., Reme, H., & Dandouras, I. (2013). Slow magnetosonic waves detected in reconnection diffusion region in the Earth's magnetotail. *Journal of Geophysical Research: Space Physics*, *118*(4), 1659–1666. <https://doi.org/10.1002/jgra.50246>
- Cartwright, M. L., & Moldwin, M. B. (2010). Heliospheric evolution of solar wind small-scale magnetic flux ropes. *Journal of Geophysical Research*, *115*(A8), A08102. <https://doi.org/10.1029/2009JA014271>
- Connerney, J. E. P. (2024). MAVEN MAG calibrated data bundle. NASA Planetary Data System. <https://doi.org/10.17189/1414251>
- Connerney, J. E. P., Espley, J., Lawton, P., Murphy, S., Odom, J., Oliverson, R., & Sheppard, D. (2015). The MAVEN magnetic field investigation. *Space Science Reviews*, *195*(1–4), 257–291. <https://doi.org/10.1007/s11214-015-0169-4>
- Cross, M. A., & Van Hoven, G. (1971). Magnetic and gravitational energy release by resistive instabilities. *Physical Review A*, *4*(6), 2347–2353. <https://doi.org/10.1103/physreva.4.2347>
- DeHoffmann, F., & Teller, E. (1950). Magneto-hydrodynamic shocks. *Physical Review*, *80*(4), 692–703. <https://doi.org/10.1103/PhysRev.80.692>
- Dong, Y., Fang, X., Brain, D. A., McFadden, J. P., Halekas, J. S., Connerney, J. E., et al. (2015). Strong plume fluxes at Mars observed by MAVEN: An important planetary ion escape channel. *Geophysical Research Letters*, *42*(21), 8942–8950. <https://doi.org/10.1002/2015GL065346>
- Dubinin, E., Fraenz, M., Fedorov, A., Lundin, R., Edberg, N., Duru, F., & Vaisberg, O. (2011). Ion energization and escape on Mars and Venus. *Space Science Reviews*, *162*(1–4), 173–211. <https://doi.org/10.1007/s11214-011-9831-7>
- Dubinin, E., Fraenz, M., Pätzold, M., Woch, J., McFadden, J., Fan, K., et al. (2020). Impact of Martian crustal magnetic field on the ion escape. *Journal of Geophysical Research: Space Physics*, *125*(10), e2020JA028010. <https://doi.org/10.1029/2020JA028010>
- Fan, K., Feaenz, M., Wei, Y., Cui, J., Rong, Z. J., Chai, L. H., & Dubinin, E. (2020). Deflection of global ion flow by the Martian crustal magnetic fields. *The Astrophysical Journal Letters*, *898*(2), L54. <https://doi.org/10.3847/2041-8213/aba519>
- Fang, X. H., Liemohn, M. W., Nagy, A. F., Luhmann, J. G., & Ma, Y. J. (2010). On the effect of the martian crustal magnetic field on atmospheric erosion. *Icarus*, *206*(1), 130–138. <https://doi.org/10.1016/j.icarus.2009.01.012>
- Fu, H. S., Chen, F., Chen, Z. Z., Xu, Y., Wang, Z., Liu, Y. Y., et al. (2020). First measurements of electrons and waves inside an electrostatic solitary wave. *Physical Review Letters*, *124*(9), 095101. <https://doi.org/10.1103/PhysRevLett.124.095101>
- Fu, H. S., Grigorenko, E. E., Gabrielse, C., Liu, C., Lu, S., Hwang, K.-J., et al. (2020). Magnetotail dipolarization fronts and particle acceleration: A review. *Science China Earth Sciences*, *63*(2), 235–256. <https://doi.org/10.1007/s11430-019-9551-y>
- Fu, H. S., Khotyaintsev, Y. V., André, M., & Vaivads, A. (2011). Fermi and betatron acceleration of suprathermal electrons behind dipolarization fronts. *Geophysical Research Letters*, *38*(16), L16104. <https://doi.org/10.1029/2011GL048528>
- Fu, H. S., Khotyaintsev, Y. V., Vaivads, A., André, M., & Huang, S. Y. (2012). Electric structure of dipolarization front at sub-proton scale. *Geophysical Research Letters*, *39*(6), L06105. <https://doi.org/10.1029/2012GL051274>
- Fu, H. S., Khotyaintsev, Y. V., Vaivads, A., André, M., Sergeev, V. A., Huang, S. Y., et al. (2012). Pitch angle distribution of suprathermal electrons behind dipolarization fronts: A statistical overview. *Journal of Geophysical Research*, *117*(A12), A12221. <https://doi.org/10.1029/2012JA018141>
- Fu, H. S., Zhao, M. J., Yu, Y., & Wang, Z. (2020). A new theory for energetic electron generation behind dipolarization front. *Geophysical Research Letters*, *47*(6), e2019GL086790. <https://doi.org/10.1029/2019GL086790>
- Fu, W. D., Fu, H. S., Cao, J. B., Yu, Y., Chen, Z. Z., & Xu, Y. (2022). Formation of rolling-pin distribution of suprathermal electrons behind dipolarization fronts. *Journal of Geophysical Research: Space Physics*, *127*(1), e2021JA029642. <https://doi.org/10.1029/2021JA029642>
- Guo, Z. Z., Fu, H. S., Cao, J. B., Wang, Y. M., Ge, M., Zhou, T. Y., et al. (2024). Rapid response of Martian magnetotail to solar wind disturbance: Tianwen-1 and MAVEN joint observations. *Geophysical Research Letters*, *51*(24), e2024GL112399. <https://doi.org/10.1029/2024GL112399>
- Guo, Z. Z., Fu, H. S., Cao, J. B., Yu, Y., Chen, Z. Z., Xu, Y., et al. (2021). Broadband electrostatic waves behind dipolarization front: Observations and analyses. *Journal of Geophysical Research: Space Physics*, *126*(12), e2021JA029900. <https://doi.org/10.1029/2021JA029900>
- Guo, Z. Z., Liu, Y. Y., Wang, Z., & Xu, Y. (2023). Energetic electron pitch-angle distributions in the martian space environment: Pancake. *The Astrophysical Journal*, *950*(1), 54. <https://doi.org/10.3847/1538-4357/acb57>
- Halekas, J. S. (2024). MAVEN SWIA calibrated data bundle. NASA Planetary Data System. <https://doi.org/10.17189/1414248>
- Halekas, J. S., Eastwood, J. P., Brain, D. A., Phan, T. D., Øieroset, M., & Lin, R. P. (2009). In situ observations of reconnection Hall magnetic fields at Mars: Evidence for ion diffusion region encounters. *Journal of Geophysical Research*, *114*(A11), A11204. <https://doi.org/10.1029/2009JA014544>
- Halekas, J. S., Taylor, E. R., Dalton, G., Johnson, G., Curtis, D. W., McFadden, J. P., et al. (2015). The solar wind ion analyzer for MAVEN. *Space Science Reviews*, *195*(1), 125–151. <https://doi.org/10.1007/s11214-013-0029-z>
- Harada, Y., Halekas, J. S., DiBraccio, G. A., Xu, S., Espley, J., McFadden, J. P., et al. (2018). Magnetic reconnection on dayside crustal magnetic fields at Mars: MAVEN observations. *Geophysical Research Letters*, *45*(10), 4550–4558. <https://doi.org/10.1002/2018GL077281>
- Harada, Y., Halekas, J. S., McFadden, J. P., Espley, J., DiBraccio, G. A., Mitchell, D. L., et al. (2017). Survey of magnetic reconnection signatures in the Martian magnetotail with MAVEN. *Journal of Geophysical Research: Space Physics*, *122*(5), 5114–5131. <https://doi.org/10.1002/2017JA023952>
- Jakosky, B. M., Lin, R. P., Grebowsky, J. M., Luhmann, J. G., Mitchell, D. F., Beutelschies, G., et al. (2015). The Mars atmosphere and volatile evolution (MAVEN) mission. *Space Science Reviews*, *195*(1–4), 3–48. <https://doi.org/10.1007/s11214-015-0139-x>
- Lin, Y., & Lee, L. C. (1993). Structure of reconnection layers in the magnetosphere. *Space Science Reviews*, *65*(1–2), 59–179. <https://doi.org/10.1007/BF00749762>
- Lion, S., Alexandrova, O., & Zaslavsky, A. (2016). Coherent events and spectral shape at ion kinetic scales in the fast solar wind turbulence. *The Astrophysical Journal*, *824*(1), 47. <https://doi.org/10.3847/0004-637X/824/1/47>
- Liu, K., Hao, X. J., Li, Y. R., Zhang, T. L., Pan, Z. H., Chen, M. M., et al. (2020). Mars orbiter magnetometer of China's first Mars mission Tianwen-1. *Earth and Planetary Physics*, *4*(4), 384–389. <https://doi.org/10.26464/epp2020058>
- MacBride, B. T., Smith, C. W., & Forman, M. A. (2008). The turbulent cascade at 1 AU: Energy transfer and the third-order scaling for MHD. *The Astrophysical Journal*, *679*(2), 1644–1660. <https://doi.org/10.1086/529575>
- Madanian, H., Halekas, J. S., Mazelle, C., Omid, N., Espley, J. R., Mitchell, D. L., & McFadden, J. P. (2020). Magnetic holes upstream of the martian bow shock: MAVEN observations. *Journal of Geophysical Research: Space Physics*, *125*(1), e2019JA027198. <https://doi.org/10.1029/2019JA027198>
- Mariani, F., Bavassano, B., & Villante, U. (1983). A statistical study of MHD discontinuities in the inner solar system: Helios 1 and 2. *Solar Physics*, *83*(2), 349–365. <https://doi.org/10.1007/BF00148285>
- Mazelle, C., Cao, J. B., Belmont, G., Neubauer, F. M., & Coates, A. J. (1997). Compressive character of low frequency waves driven by newborn ions at comet Grigg-Skjellerup. *Advances in Space Research*, *20*(2), 267–270. [https://doi.org/10.1016/S0273-1177\(97\)00544-9](https://doi.org/10.1016/S0273-1177(97)00544-9)

- Mazelle, C., Winterhalter, D., Sauer, K., Trotignon, J. G., Acuna, M. H., Baumgartel, K., et al. (2004). Bow shock and upstream phenomena at Mars. *Space Science Reviews*, *111*(1/2), 115–181. <https://doi.org/10.1023/B:SPAC.0000032717.98679.d0>
- Mitchell, D. L. (2024). *MAVEN SWEA calibrated data bundle*. NASA Planetary Data System. <https://doi.org/10.17189/1414254>
- Mitchell, D. L., Mazelle, C., Sauvaud, J. A., Thocaven, J. J., Rouzaud, J., Fedorov, A., et al. (2016). The MAVEN solar wind electron analyzer. *Space Science Reviews*, *200*(1–4), 495–528. <https://doi.org/10.1007/s11214-015-0232-1>
- Modolo, R., Chanteur, G. M., & Dubinin, E. (2012). Dynamic Martian magnetosphere: Transient twist induced by a rotation of the IMF. *Geophysical Research Letters*, *39*(1), L01106. <https://doi.org/10.1029/2011GL049895>
- Nagy, A. F., Winterhalter, D., Sauer, K., Cravens, T. E., Brecht, S., Mazelle, C., et al. (2004). The plasma environment of Mars. *Space Science Reviews*, *111*(1/2), 33–114. <https://doi.org/10.1023/B:SPAC.0000032718.47512.92>
- Ramstad, R., Brain, D. A., Dong, Y. X., Espley, J., Halekas, J., & Jakosky, B. (2020). The global current systems of the Martian induced magnetosphere. *Nature Astronomy*, *4*(10), 979–985. <https://doi.org/10.1038/s41550-020-1099-y>
- Smith, E. J. (1973). Identification of interplanetary tangential and rotational discontinuities. *Journal of Geophysical Research*, *78*(13), 2054–2063. <https://doi.org/10.1029/JA078i013p02054>
- Song, P., & Russell, C. (1999). Time series data analyses in space physics. *Space Science Reviews*, *87*(3/4), 387–463. <https://doi.org/10.1023/A:1005035800454>
- Sonnerup, B. U., & Cahill, L. J., Jr. (1968). Explorer 12 observations of the magnetopause current layer. *Journal of Geophysical Research*, *73*(5), 1757–1770. <https://doi.org/10.1029/JA073i005p01757>
- Sonnerup, B. U. Ö., Haaland, S., Paschmann, G., Dunlop, M. W., Rème, H., & Balogh, A. (2006). Orientation and motion of a plasma discontinuity from single-spacecraft measurements: Generic residue analysis of Cluster data. *Journal of Geophysical Research*, *111*(A5), A05203. <https://doi.org/10.1029/2005JA011538>
- Sonnerup, B. U. Ö., Haaland, S. E., Paschmann, G., & Denton, R. E. (2018). Quality measure for the Walén relation. *Journal of Geophysical Research: Space Physics*, *123*(12), 9979–9990. <https://doi.org/10.1029/2018JA025677>
- Tessein, J. A., Matthaeus, W. H., Wan, M., Osman, K. T., Ruffolo, D., & Giacalone, J. (2013). Association of suprathermal particles with coherent structures and shocks. *The Astrophysical Journal Letters*, *776*(1), L8. <https://doi.org/10.1088/2041-8205/776/1/L8>
- Trotignon, J., Mazelle, C., Bertucci, C., & Acuña, M. (2006). Martian shock and magnetic pile-up boundary positions and shapes determined from the Phobos 2 and Mars Global Surveyor data sets. *Planetary and Space Science*, *54*(4), 357–369. <https://doi.org/10.1016/j.pss.2006.01.003>
- Uzdensky, D. A., & Loureiro, N. F. (2016). Magnetic reconnection onset via disruption of a forming current sheet by the tearing instability. *Physical Review Letters*, *116*(10), 105003. <https://doi.org/10.1103/PhysRevLett.116.105003>
- Wan, W. X., Wang, C., Li, C. L., & Wei, Y. (2020). China's first mission to Mars. *Nature Astronomy*, *4*(7), 721. <https://doi.org/10.1038/s41550-020-1148-6>
- Wang, G. Q., Xiao, S. D., Wu, M. Y., Zhao, Y. D., Jiang, S., Pan, Z. H., et al. (2024). Calibration of the zero offset of the fluxgate magnetometer on board the Tianwen-1 orbiter in the Martian magnetosheath. *Journal of Geophysical Research: Space Physics*, *129*(1), e2023JA031757. <https://doi.org/10.1029/2023JA031757>
- Wang, J., Pu, Z. Y., Zhou, X. Z., Zhang, X. G., Malcom, W. D., Fu, S. Y., et al. (2008). Coordinated Cluster/Double Star observations of dayside flux transfer events on 6 April 2004. *Science in China - Series E: Technological Sciences*, *51*(10), 1611–1619. <https://doi.org/10.1007/s11431-008-0265-8>
- Wang, Y. M. (2024). *Calibrated magnetic field data from MOMAG of Tianwen-1*. Solar-Terrestrial Exploration and Physics at University of Science and Technology of China. Retrieved from [https://space.ustc.edu.cn/dreams/tw1\\_momag/?magdata=cal](https://space.ustc.edu.cn/dreams/tw1_momag/?magdata=cal)
- Wang, Y. M., Zhang, T. L., Wang, G. Q., Xiao, S. D., Zou, Z. X., Cheng, L., et al. (2023). The Mars orbiter magnetometer of Tianwen-1: In-flight performance and first science results. *Earth and Planetary Physics*, *7*(2), 1–13. <https://doi.org/10.26464/epp2023028>
- Webster, L., Vainchtein, D., & Artemyev, A. (2021). Solar wind discontinuity interaction with the bow shock: Current density growth and Dawn-Dusk asymmetry. *Solar Physics*, *296*(6), 87. <https://doi.org/10.1007/s11207-021-01824-2>
- Xu, S., Curry, S. M., Mitchell, D. L., Luhmann, J. G., Lillis, R. J., & Dong, C. (2020). Suprathermal electron deposition on the Mars nightside during ICMs. *Journal of Geophysical Research: Space Physics*, *125*(10), e2020JA028430. <https://doi.org/10.1029/2020JA028430>
- Xu, Y., Fu, H., Cao, J., Liu, C., Norgren, C., & Chen, Z. (2021). Electron-scale measurements of antipolarization front. *Geophysical Research Letters*, *48*(6), e2020GL092232. <https://doi.org/10.1029/2020GL092232>
- Xu, Y., Fu, H. S., Norgren, C., Toledo-Redondo, S., Liu, C. M., & Dong, X. C. (2019). Ionospheric cold ions detected by MMS behind dipolarization fronts. *Geophysical Research Letters*, *46*(14), 7883–7892. <https://doi.org/10.1029/2019GL083885>
- Zhang, T. L., Schwingenschuh, K., Russell, C. T., & Luhmann, J. G. (1991). Asymmetries in the location of the Venus and Mars bow shock. *Geophysical Research Letters*, *18*(2), 127–129. <https://doi.org/10.1029/90GL02723>
- Zou, Z. X., Wang, Y. M., Zhang, T. L., Wang, G. Q., Xiao, S. D., Pan, Z. H., et al. (2023). In-flight calibration of the magnetometer on the Mars orbiter of Tianwen-1. *Science China Technological Sciences*, *66*(8), 2396–2405. <https://doi.org/10.1007/s11431-023-2401-2>